

## Expanding the Scope of Diamond Surface Chemistry: Stille and Sonogashira Cross-Coupling Reactions

Peer-reviewed author version

RAYMAKERS, Jorne; Artemenko, Anna; NICLEY, Shannon; Stenclova, Pavla; Kromka, Alexander; HAENEN, Ken; MAES, Wouter & Rezek, Bohuslav (2017) Expanding the Scope of Diamond Surface Chemistry: Stille and Sonogashira Cross-Coupling Reactions. In: JOURNAL OF PHYSICAL CHEMISTRY C, 121(42), p. 23446-23454.

DOI: 10.1021/acs.jpcc.7b06426

Handle: <http://hdl.handle.net/1942/25557>

# Expanding the Scope of Diamond Surface Chemistry: Stille & Sonogashira Cross-Coupling Reactions

*Jorne Raymakers<sup>1</sup>, Anna Artemenko<sup>2</sup>, Shannon S. Nicley<sup>1</sup>, Pavla Štenclová<sup>2</sup>, Alexander Kromka<sup>2</sup>, Ken Haenen<sup>1</sup>, Wouter Maes<sup>1,\*</sup>, Bohuslav Rezek<sup>2,3,\*</sup>*

<sup>1</sup> UHasselt – Hasselt University, Institute for Materials Research (IMO) & IMEC vzw,  
IMOMEC, 3590 Diepenbeek, Belgium

<sup>2</sup> Institute of Physics, Czech Academy of Sciences, Cukrovarnická 10, 162 00 Prague 6,  
Czech Republic

<sup>3</sup> Faculty of Electrical Engineering, Czech Technical University in Prague, Technická 2, 166  
25 Prague 6, Czech Republic

## Abstract

Well-defined covalent surface functionalization of diamond is a crucial, yet non-trivial, matter because of diamonds intrinsic chemical inertness and stability. Herein, we demonstrate a two-step functionalization approach for H-terminated boron-doped diamond thin films, which can lead to significant advances in the field of diamond hybrid photovoltaics. Primary diamond surface functionalization is performed via electrochemical diazonium grafting of *in situ* diazotized 4-iodoaniline. The freshly grafted iodophenyl functional moieties are then employed to couple a layer of thiophene molecules to the diamond surface via two well-established Pd-catalyzed cross-coupling reactions, i.e. Stille and Sonogashira. X-ray photoelectron spectroscopy analysis indicates a dense coverage and successful cross-coupling in both cases. However, we find that the Stille reaction is generally accompanied with severe surface contamination, in spite of process optimization and thorough rinsing. Sonogashira cross-coupling on the other hand provides a clean, high quality functionalization over a broad range of reaction conditions. The protocols employing Sonogashira reactions thus appear to be the method of choice toward future fabrication of high-performance dye-functionalized diamond electrodes for photovoltaic applications.

# 1. Introduction

Since early human history, diamond is publicly known as a precious gemstone. However, its purely scientific value has strongly increased after the development of techniques such as chemical vapor deposition (CVD).<sup>1</sup> CVD allows the growth of diamond thin films on various substrates at a reasonably low temperature and with a minimized cost.<sup>2</sup> Combined with the many appealing properties of diamond, *i.e.* an extreme hardness,<sup>3</sup> high optical transparency,<sup>4</sup> excellent thermal conductivity,<sup>5</sup> a wide electrochemical potential window,<sup>6</sup> chemical inertness<sup>7</sup> and a good biocompatibility,<sup>8</sup> it has become a very attractive material from a scientific point of view.<sup>9</sup> Furthermore, synthetic diamond films show *p*-type conductivity upon doping with boron. High doping ratios can afford up to metallic conductivities with a specific resistivity as low as 0.005  $\Omega$ ,<sup>10</sup> paving the way for numerous applications. For instance, boron-doped diamond (BDD) thin films have been employed as electrodes for electro-catalytic reactions<sup>11</sup> and in (bio)sensors.<sup>12–14</sup> Because of its *p*-type conductivity,<sup>5,15</sup> BDD is also attractive as an alternative photocathode material for dye-sensitized solar cells (DSSCs).<sup>16,17</sup>

Nevertheless, one of diamonds core advantages – a chemically inert surface – also causes some important limitations and challenges. The low reactivity of the diamond surface, and H-terminated surfaces in particular, complicates direct functionalization. For the functionalization of H-terminated diamond surfaces, a two-step approach is generally required, wherein functional groups are initially introduced via spontaneous or electrochemical diazonium grafting of an (*in situ* generated) aryl diazonium salt,<sup>18–20</sup> photochemical grafting under illumination with UV light (254 nm)<sup>21,22</sup> or plasma treatment of the surface.<sup>23,24</sup> Subsequently, the freshly introduced functional handles can be employed to attach a variety of (bio)molecules utilizing several coupling reactions, such as EDC-NHS,<sup>25</sup>

thiol-ene/yne,<sup>26</sup> Cu-catalyzed azide-alkyne cycloaddition<sup>27–29</sup> or Pd-catalyzed Suzuki cross-coupling.<sup>16,30,31</sup>

By employing a combination of diazonium grafting and Pd-catalyzed Suzuki cross-coupling, organic molecules can be readily attached to the diamond surface via stable carbon-carbon bonds in a fully conjugated fashion. These developments opened up the possibility for BDD electrodes to become relevant photovoltaic materials. This was first demonstrated by Zhong *et al.* in 2008 by coupling two organic molecules, *i.e.* bithiophene-C<sub>60</sub> and bithiophene-dicyanovinyl, to a phenylboronate functionalized diamond surface.<sup>16</sup> However, extremely low currents were generated, which is related to the limited amount of organic dye molecules being coupled to the surface. Therefore, scientists are continuously looking for methods to improve the surface coverage of diamond electrodes. This can for instance be achieved by increasing the surface area of the electrodes using mesoporous diamond foams,<sup>32</sup> nanowires<sup>33</sup> or fibers<sup>34</sup> instead of regular thin films. An alternative approach is the careful optimization of existing types of diamond functionalization chemistry<sup>35</sup> or the development of novel functionalization strategies.<sup>36,37</sup> Ideally, efforts in both directions are combined, which has recently led to the development of a champion BDD foam electrode generating currents of *ca.* 500–700 nA cm<sup>-2</sup> at –0.2 V bias under white light illumination.<sup>38</sup>

Despite promising results in previous research, diamond-based DSSCs are still far from being competitive with their NiO counterparts. The current NiO *p*-type DSSCs generate currents of approximately 2.0 mA cm<sup>-2</sup>, which is 4 orders of magnitude higher than the top performing diamond photocathodes.<sup>39,40</sup> This difference is even more pronounced when compared to state of the art *n*-type DSSCs.<sup>41</sup> One of the major reasons behind these low currents of diamond-based photovoltaics still remains, amongst others, the challenging surface functionalization of diamond. Hence, in this work we contribute to improving the overall diamond surface functionalization chemistry by expanding the range of reactions on a

(H-terminated) diamond surface, using a two-step protocol. Initial surface functionalization is performed via electrochemical diazonium grafting of 4-iodoaniline. During this grafting procedure, an actual carbon-carbon bond is formed between the diamond electrode and the organic compound. Apart from an improved stability compared to traditional DSSCs – having a weaker coordination bond – the charge transfer between the light-harvesting compound and the diamond electrode can be enhanced since a direct pathway is constructed. The first Pd-catalyzed reaction optimized in this work is the Stille cross-coupling, which is currently the most established reaction for C-C (aryl-aryl) bond formation in complex organic compounds and (in particular) semiconducting polymers because of its high selectivity, broad scope, tolerance toward most functional groups and excellent reaction yields.<sup>42,43</sup> For this optimization study, rather simple stannylthiophenes were employed instead of expensive dyes and the influence of the reactants, catalysts, ligands and concentration was analyzed. Additionally, the Sonogashira cross-coupling was examined as well, since the (hetero)arylethynyl derivatives are more easily prepared and purified than their stannyl analogues.<sup>44</sup> Apart from maximizing the surface coverage, a second key factor in obtaining efficient diamond photovoltaics is to minimize the presence of surface impurities. With this in mind, the diamond surface was analyzed by X-ray photoelectron spectroscopy (XPS) during the screening of the optimal reaction conditions for both the Stille and Sonogashira cross-coupling protocols.

## **2. Experimental Section**

### **2.1 Materials**

All purchased chemicals were of the highest quality and they were used without further purification. Sodium nitrate, 4-iodoaniline, 2-ethynylthiophene, 2-dicyclohexylphosphino-2',6'-dimethoxybiphenyl (SPhos), 2-dicyclohexylphosphino-2',4',6'-triisopropylbiphenyl (XPhos) and copper(I) iodide were purchased from Sigma-Aldrich. Triethylamine (TEA),

diisopropylamine (DIPA), dry toluene, dry *N,N*-dimethylformamide (DMF) and dry tetrahydrofuran (THF) were purchased from Acros Organics. 2-(Tributylstannyl)thiophene was purchased from J&K Scientific. Tris(dibenzylideneacetone)dipalladium(0), tetrakis(triphenylphosphine)palladium(0), tri(*ortho*-tolyl)phosphine, *trans*-dichlorobis(triphenylphosphine)palladium(II) and palladium(II) acetate were purchased from Strem Chemicals. All solvents employed for rinsing were of HPLC grade.

## 2.2 Synthesis

**Trimethyl(thiophen-2-yl)stannane:** A solution of *n*-BuLi in *n*-hexane (2.5 M; 8.10 mL) was added dropwise to a solution of 2-bromothiophene (18.4 mmol, 3.00 g) in dry THF (30 mL) at  $-78\text{ }^{\circ}\text{C}$ . After stirring for 1 h at this temperature, a solution of trimethyltin chloride in THF (1.0 M; 22.1 mL) was added rapidly at  $-78\text{ }^{\circ}\text{C}$ . The reaction mixture was brought to room temperature and after stirring overnight, diethyl ether (100 mL) was added. The mixture was washed with water (3 x 75 mL) and brine (75 mL), dried over  $\text{MgSO}_4$ , filtered and concentrated *in vacuo*. The crude product was purified by a combination of preparative gel permeation chromatography and Kugelrohr ( $60\text{ }^{\circ}\text{C}$ , 5 mbar), yielding the product as a colorless oil (2.15 g, 47%).  $^1\text{H}$  NMR (400 MHz,  $\text{CDCl}_3$ ,  $\delta$ ): 7.68–6.62 (m, 1H), 7.28–7.21 (m, 2H), 0.37 (s, 9H).<sup>45</sup>

**4-Iodobenzenediazonium chloride:** 4-Iodoaniline (10.9 mg, 50  $\mu\text{mol}$ ) was diazotized 5 min prior to the electrografting protocol by adding an equimolar amount of  $\text{NaNO}_2$  (3.45 mg, 50  $\mu\text{mol}$ ). 4-Iodoaniline was dissolved in an Ar-purged HCl solution (0.5 M; 9.5 mL) and a  $\text{NaNO}_2$  solution (0.1 M; 0.5 mL) in HCl (0.5 M) was added, resulting in a final concentration of 5 mM. After vigorously shaking the solution, it was used for electrochemical grafting via cyclic voltammetry.

## 2.3 Diamond Growth

150 nm thick B:NCD films were grown on (100)-oriented 10 mm x 10 mm Si *p*-type conductive substrates by microwave plasma enhanced chemical vapor deposition (MWPECVD), with trimethylborane (TMB) as the boron source.<sup>46</sup> Characterization performed on samples grown in the same reactor under similar growth conditions indicate that the B:NCD films have boron concentrations of approximately  $5 \times 10^{21} \text{ cm}^{-3}$  and resistivity ( $\rho$ ) below  $5 \text{ m}\Omega \text{ cm}$ .<sup>5,46</sup> For FTIR analysis, a 190 nm B:NCD film was grown on an Au mirror on a 10 mm x 10 mm Corning Eagle glass substrate. Full details of the deposition processes and field emission gun - scanning electron microscope (FEG-SEM) images are given in the Supporting Information.

## 2.4 Diazonium Electrografting

The B:NCD surfaces were functionalized with 4-iodophenyl moieties by means of electrochemical diazonium grafting of the *in situ* generated 4-iodobenzenediazonium chloride with cyclic voltammetry.<sup>28</sup> The electrografting reactions were performed with an Autolab PGSTAT30 potentiostat (Eco Chemie B.V.) and were controlled by the GPES Manager program. A one-compartment electrochemical cell was used in a three-electrode configuration. Hydrogen-terminated B:NCD was employed as the working electrode, a platinum wire as the counter electrode and a Ag/AgCl/KCl(sat) electrode as the reference. All potentials are reported versus this reference electrode at room temperature. Diamond working electrodes were functionalized in two steps by immersing each half of the sample in the *in situ* generated 4-iodobenzenediazonium chloride solution. Optimization of the electrografting process was performed by cyclic voltammetry scanning at two different potentials (+500 to -1500 mV and +500 to -600 mV vs. Ag/AgCl) at a scan rate of  $100 \text{ mV s}^{-1}$  for ten scans. After grafting, the B:NCD samples were sonicated in MiliQ water and subsequently rinsed



with ultrapure *n*-hexane, tetrahydrofuran, ethanol and MiliQ water before drying with a nitrogen flow.

## 2.5 Palladium-Catalyzed Cross-Coupling

All Stille and Sonogashira cross-coupling reaction mixtures were prepared in a glovebox to ensure an inert atmosphere. In all cases, a schlenk vial equipped with a stirring bar was loaded with the Pd source, ligand, diamond substrate, thiophene derivative and solvent (and base and CuI in case of the Sonogashira reactions). The vial was then closed off with a rubber septum, removed from the glovebox and placed in an oil bath at 110 or 60 °C for the Stille and Sonogashira cross-coupling reactions, respectively. After the cross-coupling, all B:NCD samples were subsequently sonicated in ultrapure *n*-hexane, acetone, ethanol and MiliQ water before drying with a nitrogen flow. Detailed information on the employed reaction conditions can be found in the footnotes to the Tables 1–4.

## 2.6 XPS Analysis

The chemical composition of the diamond surfaces was analyzed by X-ray photoelectron spectroscopy using an XPS spectrometer (Kratos, AXIS Supra) equipped with a hemispherical analyzer and a monochromatic AlK $\alpha$  X-ray source (1486.6 eV). The XPS spectra were acquired from an area of 0.7  $\times$  0.3 mm<sup>2</sup> with a take-off angle of 90°. The survey XPS spectra were recorded with a pass energy of 80 eV, whereas the high-resolution spectrum scans were recorded with a pass energy of 20 eV. The obtained XPS spectra were calibrated on 283.8 eV binding energy (sp<sup>3</sup> carbon phase).<sup>47</sup> The CasaXPS software with implemented linear baseline and Gaussian line shapes was used for spectra processing. XPS peak positions were determined with an accuracy of  $\pm 0.2$  eV. The high resolution S 2p peaks were decomposed into three different peaks with binding energies of 163.9 (S 2p<sub>3/2</sub>), 165.0 (S 2p<sub>1/2</sub>) and 168.5 eV (SO<sub>x</sub>), respectively.<sup>48,49</sup> The weak peak located at 168.5 eV is attributed to oxidized sulfur groups.

## 2.7 FTIR Analysis

GAR-FTIR (grazing angle reflectance Fourier transform infrared) spectra were measured using a N<sub>2</sub>-purged Thermo Nicolet 870 spectrometer equipped with a KBr beam splitter and an MCT detector cooled by liquid nitrogen. The optical absorbance was calculated in standard absorbance units as  $A = -\log(R/R_0)$ , where R is the spectrum of the analyzed material and R<sub>0</sub> is the reference (background) spectrum recorded using a 190 nm B:NCD thin film that was grown on an Au mirror on a 10 x 10 mm Corning Eagle glass substrate (details provided in Supporting Information). In all cases, the spectra represent an average of 128 scans recorded with a resolution of 4 cm<sup>-1</sup>.

## 2.8 Electrochemical oxidation thiophene

Sonogashira cross-coupling of the iodophenyl functionalized B:NCD surface with 2-ethynylthiophene was confirmed by cyclic voltammetry using an Autolab PGSTAT30 potentiostat (Eco Chemie B.V.), controlled by the GPES Manager program. A one-compartment electrochemical cell was used in a three-electrode configuration. Thienyl functionalized B:NCD was employed as the working electrode, a platinum wire as the counter electrode and a Ag/AgNO<sub>3</sub> electrode as the reference (silver wire dipped in a solution of 0.01 M AgNO<sub>3</sub> and 0.1 M NBu<sub>4</sub>PF<sub>6</sub> in anhydrous acetonitrile). All potentials are reported versus this reference electrode at room temperature. Oxidation of the thienyl moieties was performed by partially submerging the electrode in a solution of 0.1 M NBu<sub>4</sub>PF<sub>6</sub> in anhydrous acetonitrile and cycling the potential between 0 and +1500 mV vs. AgNO<sub>3</sub> at a scan rate of 100 mV s<sup>-1</sup> for five scans.

### 3. Results & Discussion

#### 3.1. Electrochemical Diazonium Grafting of a 4-Iodophenyl Layer

Initial surface functionalization of a H-terminated boron-doped nanocrystalline diamond (B:NCD) thin film was performed via the electrochemical diazonium grafting of 4-iodobenzenediazonium chloride, as shown in Scheme 1. The diazonium salt was generated via the *in situ* diazotization of a solution of 4-iodoaniline in hydrochloric acid by adding an equimolar amount of sodium nitrate. 4-Iodoaniline was chosen over 4-bromoaniline as the subsequent Pd-catalyzed reactions typically show higher efficiencies due to improved oxidative addition rates. Additionally, it can also be expected that the “bulkiness” of the iodine groups might hinder the formation of multilayers to some extent, as was demonstrated for the grafting of trimethylsilyl-protected 4-ethynylaniline.<sup>50</sup>

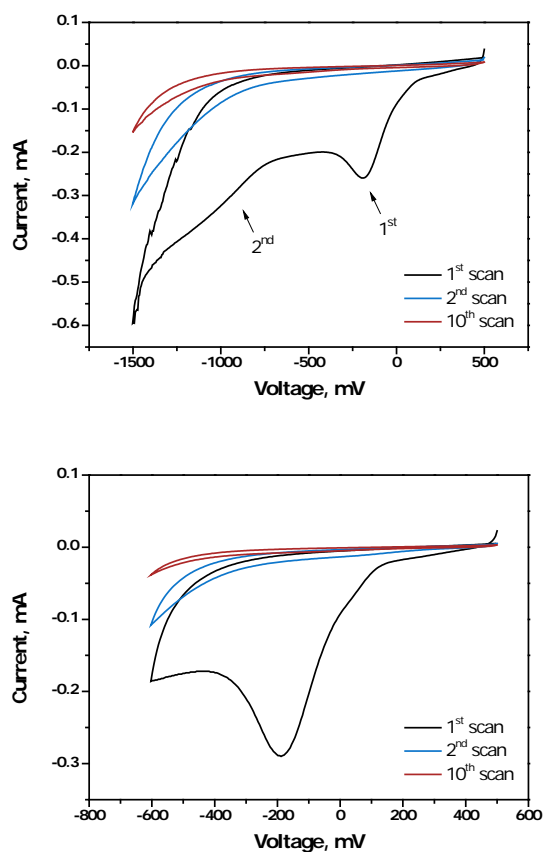


**Scheme 1.** Overall strategy for the functionalization of H-terminated B:NCD: (i) *In situ* diazotization; (ii) Electrochemical reduction of the corresponding diazonium salt; (iii) Pd-catalyzed Stille (a) and Sonogashira (b) cross-coupling using 2-(trimethylstannyl)thiophene or 2-ethynylthiophene, respectively.

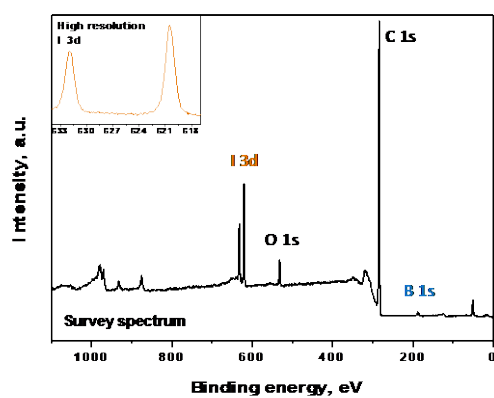
To get a general idea on the behavior of 4-iodoaniline during the electrochemical grafting procedure, a broad potential scan from +500 to –1500 mV (versus an Ag/AgCl reference electrode) was initially performed. This was done by immersing a homegrown B:NCD

working electrode in an aqueous (HCl) solution of the mentioned diazonium salt while cycling to a reductive potential. From the cyclic voltammogram (Figure 1, top), one can clearly see a first broad irreversible reduction peak at  $-190$  mV, which corresponds with the electroreduction of the diazonium salt, resulting in the formation of phenyl radicals. However, upon reaching a more negative potential of approximately  $-850$  mV, a second reduction peak appears, which relates to further reduction of the previously generated aryl radicals to anions.<sup>19</sup> Since the formation of anions is an undesired process for the diazonium grafting procedure, a second potential scan was run from  $+500$  to  $-600$  mV (Figure 1, bottom). Here, only a reduction of the diazonium salt to the corresponding radical was observed during the first scan. In subsequent scans, the reduction peak disappeared, indicating successful grafting of the envisaged iodophenyl layer, which leads to passivation of the diamond surface.

Functionalization of the B:NCD thin films with iodophenyl groups was then confirmed by XPS. The corresponding I 3d signals appear in the survey spectrum at  $627$  eV (Figure 2, top). Integration of the I 3d peak revealed a mean relative iodine concentration (measured over 4 samples) on the diamond surface of  $0.6 \pm 0.1$  at.% (Table S1). However, it should be noted that the attenuation length of the employed X-rays ( $1486.6$  eV) is approximately  $3.5$  nm for carbon.<sup>51</sup> Therefore, the iodine concentration on the topmost surface is significantly higher. Considering the thickness of one carbon layer vs. the whole volume probed by XPS, one can estimate an increase by about one order of magnitude, which then yields  $6$  at.% of iodine on the topmost surface. This is similar to the  $5\%$  coverage reported for dense diazonium layers electrochemically grafted to BDD.<sup>52</sup> Additionally, Fourier transform infrared (FTIR) spectroscopy (Figure 2, bottom) revealed a signal related to the C-H stretch vibrations of the aromatic rings at  $3011$   $\text{cm}^{-1}$ . The signal at  $2270$   $\text{cm}^{-1}$  can likely be attributed to aromatic overtones.<sup>53</sup>



**Figure 1.** Cyclic voltammograms showing the electrochemical grafting of *in situ* generated 4-iodobenzenediazonium chloride on H-terminated B:NCD thin films with applied potentials between + 500 and –1500 mV (top) or between + 500 and –600 mV (bottom) at a scan rate of  $100 \text{ mV s}^{-1}$  for 10 scans.



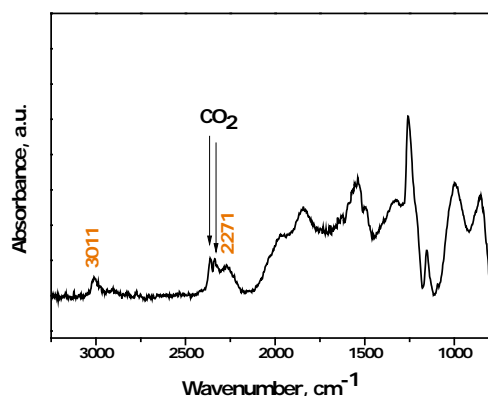


**Figure 2.** XPS survey spectrum (top) and FTIR spectrum (bottom) of an iodophenyl functionalized B:NCD thin film.

### 3.2. Palladium-Catalyzed Cross-Coupling Reactions: Stille & Sonogashira

The iodine functionalized diamond surface provides an excellent platform for further functionalization via Pd-catalyzed cross-couplings. Accordingly, a broad range of reaction conditions, *i.e.* catalysts, ligands and organostannyl reagents, were screened for the Stille cross-coupling reaction (Table 1, 2). The resulting coupling efficiencies were analyzed by means of XPS. For this optimization study, two simple stannylthiophene derivatives, 2-(trimethylstannyl)thiophene and 2-(tributylstannyl)thiophene, were selected as model compounds as they are inexpensive and more easily synthesized when compared to the more complex light-harvesting molecules required for the final photovoltaic devices. 2-(Trimethylstannyl)thiophene was synthesized from 2-bromothiophene via the generation of an organolithium derivative and subsequent reaction with trimethyltin chloride.<sup>45</sup> 2-(Tributylstannyl)thiophene is commercially available and has a somewhat lower reaction rate compared to the methyl variant for steric reasons.<sup>54</sup> This lower reactivity is, however, compensated by a higher stability. Through this initial screening using relatively simple catalyst/ligand systems, the balance between reactivity and stability of the organostannyl reagents was investigated.

**Table 1.** Optimization of the Stille cross-coupling conditions on B:NCD thin films through analysis of the chemical composition of the diamond surface by XPS: (i) 2-(trimethylstannyl)thiophene versus 2-(tributylstannyl)thiophene.

Entry	Catalyst/Ligand	Reagent	O at. %	C at. %	B at. %	Pd at. %	S at. %	Sn at. %
1	Pd(PPh <sub>3</sub> ) <sub>4</sub> (6 mol%)	2-(trimethylstannyl)thiophene	16	73	5	4	1	1
2	Pd(PPh <sub>3</sub> ) <sub>4</sub> (6 mol%)	2-(tributylstannyl)thiophene	46	3	-	11	2	10
3	Pd(PPh <sub>3</sub> ) <sub>2</sub> Cl <sub>2</sub> (6 mol%)	2-(trimethylstannyl)thiophene	12	79	4	2	1	2
4	Pd(PPh <sub>3</sub> ) <sub>2</sub> Cl <sub>2</sub> (6 mol%)	2-(tributylstannyl)thiophene	29	58	-	6	2	5
5	Pd <sub>2</sub> dba <sub>3</sub> (3 mol%) / P( <i>o</i> -tolyl) <sub>3</sub> (12 mol%)	2-(trimethylstannyl)thiophene	8	85	4	1	1	1
6	Pd <sub>2</sub> dba <sub>3</sub> (3 mol%) / P( <i>o</i> -tolyl) <sub>3</sub> (12 mol%)	2-(tributylstannyl)thiophene	26	58	-	7	1	8

General reaction conditions: 0.1 mmol stannyl reagent, dry toluene (6 mL), dry DMF (2 mL), 110 °C, 18 h.

Table 1 shows the employed reaction conditions and the relative atomic concentrations of the different chemical elements on the diamond surface after reaction, as obtained by XPS analysis of the functionalized BDD films. The sulfur concentration was calculated based on the intensity of the S 2p signal in the survey spectrum and was used for comparing the efficiency of the coupling reactions. Furthermore, the detected Pd 3d and Sn 3d signals were employed to estimate the surface contamination, whereas the B 1s signal gives an indication of the layer thickness on top of the diamond film. Since the penetration depth of an X-ray beam is limited to a few nanometers, a very thick surface layer results in disappearance of the boron signal, whereas thinner layers still allow B 1s detection. Based on the results, it appears that for the three different catalyst systems (Table 1), larger Pd and Sn contaminations are obtained when employing 2-(tributylstannyl)thiophene, even after thorough rinsing of the samples. Additionally, the B 1s signal was no longer detectable in the XPS survey spectrum for reactions employing 2-(tributylstannyl)thiophene. This indicates that rather thick and highly contaminated layers are obtained. Hence, the Stille cross-coupling on a B:NCD thin film is strongly influenced by sterical hindrance of the reagents and proceeds significantly better when using more reactive, less bulky organostannyl derivatives.

To further improve the coupling reaction and decrease the amount of contamination, electron rich and sterically hindered catalyst systems, developed by the Buchwald group, were investigated.<sup>55</sup> These catalyst systems typically comprise Pd(OAc)<sub>2</sub> or Pd<sub>2</sub>dba<sub>3</sub> as the palladium source and a monodentate biarylphosphine ligand such as 2-dicyclohexylphosphino-2',6'-dimethoxybiphenyl (SPhos) or 2-dicyclohexylphosphino-2',4',6'-triisopropylbiphenyl (XPhos), facilitating the oxidative addition step due to their electron rich nature.<sup>56</sup> Moreover, as the ligands are relatively bulky, only a 12-electron Pd complex will be formed in the transition state, resulting in a higher reactivity and faster reductive elimination.<sup>55</sup> Similar catalyst systems have previously been used to optimize the Suzuki cross-coupling of light-harvesting molecular wires on B:NCD films.<sup>35</sup> Encouraged by these results, some of these conditions were also applied for the Stille functionalization of B:NCD (Table 2).

**Table 2.** Optimization of the Stille cross-coupling conditions on B:NCD thin films through analysis of the chemical composition of the diamond surface by XPS: (ii) sterically hindered electron rich ligands.

Entry	Catalyst/Ligand	O at. %	C at. %	B at. %	Pd at. %	S at. %	Sn at. %
7	Pd(OAc) <sub>2</sub> (6 mol%) / XPhos (7 mol%)	46	31	-	13	2	8
8	Pd(OAc) <sub>2</sub> (6 mol%) / SPhos (7 mol%)	43	35	-	10	3	9
9	Pd <sub>2</sub> dba <sub>3</sub> (3 mol%) / XPhos (7 mol%)	22	67	-	6	1	4
10	Pd <sub>2</sub> dba <sub>3</sub> (3 mol%) / SPhos (7 mol%)	40	40	-	11	1	8

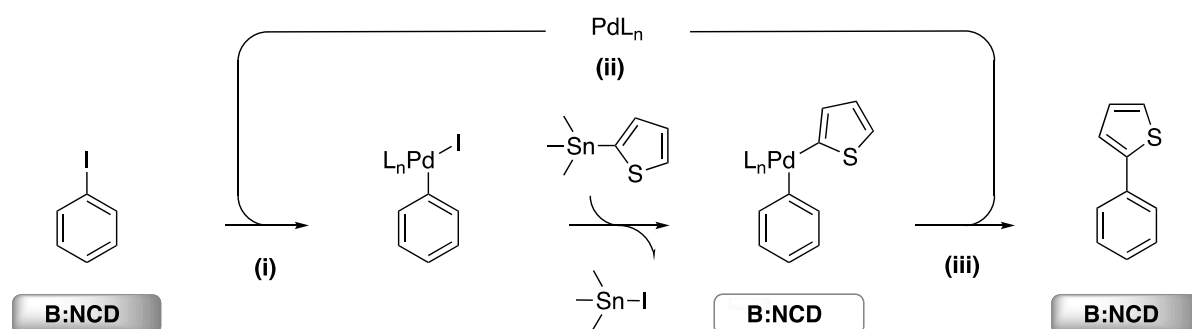
General reaction conditions: 2-(trimethylstannyl)thiophene (0.05 mmol), dry toluene (6 mL), dry DMF (2 mL), 110 °C, 18 h.

For the more advanced catalytic systems, high concentrations of Pd and Sn were always observed, while the signal corresponding to the B 1s peak was not detected. This indicates the formation of a thick contamination layer instead of a clean surface functionalization. Surprisingly, the most reactive catalyst systems give inferior results. A possible explanation



can be found in the fact that the different reactions steps of the Pd-catalyzed cross-coupling, *i.e.* oxidative addition, transmetallation and reductive elimination, are taking place on the diamond surface rather than in solution, as illustrated in Scheme 2. The rate of the oxidative addition is generally favored by employing catalyst systems with electron rich ligands, increasing in the order  $\text{PPh}_3 < \text{P}(o\text{-tolyl})_3 < \text{XPhos/SPhos}$ . On the other hand, the driving force for the reductive elimination is influenced by the stability of the generated Pd complex. More sterically hindered ligands afford complexes with a larger deviation from the most stable 18-electron configuration. Hence, the rate of reductive elimination will strongly improve.<sup>42</sup> Both XPhos and SPhos are electron rich and bulky ligands, which should favor the oxidative addition and reductive elimination steps. As a result, the problem for the Stille cross-coupling on diamond is likely to be found in the transmetallation, which is regarded as the rate-determining step in many cases.<sup>57</sup> Since the Pd complex is immobilized onto the B:NCD surface, the degree of freedom drastically decreases, rendering steric hindrance of the ligands an important factor. When relatively small ligands are used, the reaction proceeds relatively fast. However, when very bulky ligands are employed, the reaction will proceed significantly slower. Since the employed ligands are electron rich, this also facilitates oxidation of the palladium complex to palladium black, resulting in severe surface contamination.<sup>57</sup> Therefore, when performing Pd-catalyzed cross-coupling reactions on any surface, the catalyst system should be chosen in such a way that a good balance is obtained between the reaction rates of the oxidative addition, transmetallation and reductive elimination. A solution to the aforementioned problem could be the ‘inverse’ Stille reaction, where the stannyl function is situated on the diamond surface, while the Pd complex is formed on the thiophene reagent. Since the thiophene molecule in such case is still in solution, a higher degree of freedom is obtained, which can improve the Stille cross-coupling using

sterically hindered ligands (see Scheme S1). However, due to the instability of organostannyl derivatives, diazonium grafting of these compounds is rather inconvenient.



**Scheme 2.** (i) Oxidative addition, (ii) transmetalation and (iii) reductive elimination for the Stille cross-coupling on iodophenyl functionalized B:NCD surfaces.

The conditions that previously afforded the best results (Table 1, entry 5) were then further used for a small concentration screening (Table 3), aiming at a system that combines a decent surface coverage with minimal contamination. However, regardless whether higher or lower concentrations of the stannyl reagent were used, the degree of functionalization remained similar.

**Table 3.** Optimization of the Stille cross-coupling conditions on B:NCD thin films through analysis of the chemical composition of the diamond surface by XPS: (iii) influence of the concentration of 2-(trimethylstannyl)thiophene.

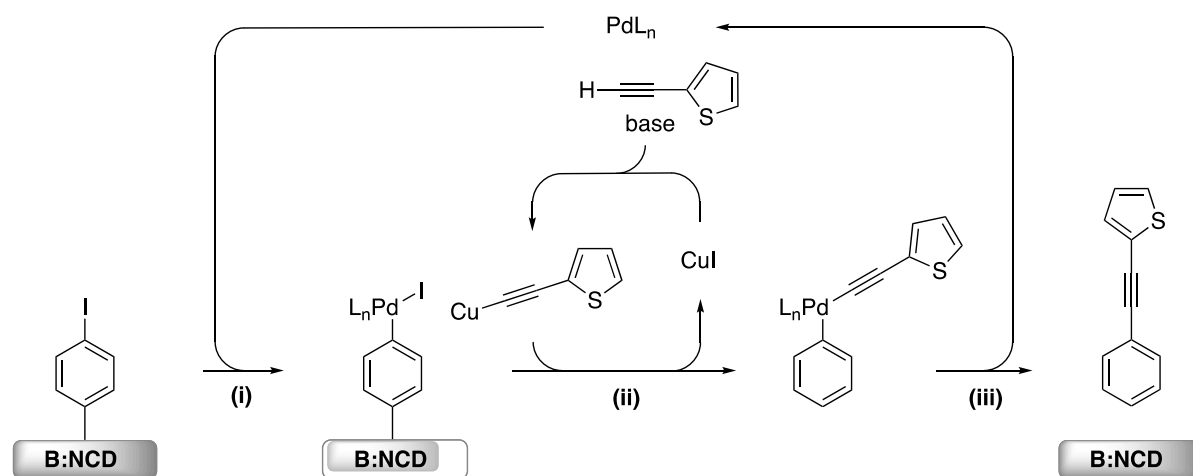
Entry	2-(Trimethylstannyl)thiophene	O at. %	C at. %	B at. %	Pd at. %	S at. %	Sn at. %
11	0.025 mmol	19	69	2	4	1	6
12	0.2 mmol	40	48	-	6	1	5

General reaction conditions: Pd<sub>2</sub>dba<sub>3</sub> (3 mol%), P(*o*-tolyl)<sub>3</sub> (12 mol%), dry toluene (6 mL), dry DMF (2 mL), 110 °C, 18 h.

Despite the fact that some thiophene coupling to the diamond surface certainly occurs, the Stille cross-coupling was found in general to be rather unreliable, resulting in pronounced surface contamination. This can partly be ascribed to the fact that relatively unstable

organotin derivatives are employed. It is assumed that over the course of the reaction these stannyl compounds degrade and precipitate onto the diamond surface.

Another attractive reaction for diamond surface functionalization is the Sonogashira cross-coupling, wherein the reaction between an organohalide and an alkyne is catalyzed using Pd and Cu is employed as a co-catalyst.<sup>44</sup> The different steps involved in the catalytic cycle of a Sonogashira reaction on the diamond surface are illustrated in Scheme 3. This reaction resembles the Stille cross-coupling, but in this case a more stable arylalkyne reagent (*in casu* 2-ethynylthiophene) is used instead of an organotin derivative. Different Sonogashira cross-coupling conditions were investigated using a combination of several catalysts, ligands and bases. Furthermore, a concentration screening was also performed (Table 4). Based on the results for the Stille cross-coupling, catalyst systems involving bulky ligands were excluded, as well as the least reactive  $\text{Pd}(\text{PPh}_3)_4$  catalyst.



**Scheme 3.** (i) Oxidative addition, (ii) transmetalation and (iii) reductive elimination for the Sonogashira cross-coupling on iodophenyl functionalized B:NCD surfaces.

**Table 4.** Optimization of the Sonogashira cross-coupling conditions on B:NCD thin films through analysis of the chemical composition of the diamond surface by XPS.

Entry	Catalyst/Ligand	Base	2-Ethynylthiophene	O at. %	C at. %	B at. %	Pd at. %	S at. %	Cu at. %	I at. %
1	Pd(PPh <sub>3</sub> ) <sub>2</sub> Cl <sub>2</sub> (5 mol%)	TEA	0.1 mmol	6.0	83.6	4.0	0.3	4.0	0.1	0.2
2	Pd(PPh <sub>3</sub> ) <sub>2</sub> Cl <sub>2</sub> (5 mol%)	DIPA	0.2 mmol	5.8	89.4	2.5	0.2	1.9	0.1	0.1
3	Pd(PPh <sub>3</sub> ) <sub>2</sub> Cl <sub>2</sub> (5 mol%)	DIPA	0.1 mmol	4.7	89	4.0	-	2.0	0.1	0.2
4	Pd(PPh <sub>3</sub> ) <sub>2</sub> Cl <sub>2</sub> (5 mol%)	DIPA	0.075 mmol	4.5	90	3.5	0.3	1.5	-	0.2
5	Pd(PPh <sub>3</sub> ) <sub>2</sub> Cl <sub>2</sub> (5 mol%)	DIPA	0.025 mmol	5.0	89.6	3.5	0.4	1.3	-	0.2
6	Pd(PPh <sub>3</sub> ) <sub>2</sub> Cl <sub>2</sub> (2.5 mol%)	DIPA	0.1 mmol	5.0	86.4	4.0	0.8	3.5	0.1	0.2
7	Pd <sub>2</sub> dba <sub>3</sub> (2.5 mol%) / P( <i>o</i> -tolyl) <sub>3</sub> (10 mol%)	TEA	0.1 mmol	5.3	84	5.0	1.0	4.0	0.2	0.5
8	Pd <sub>2</sub> dba <sub>3</sub> (1.25 mol%) / P( <i>o</i> -tolyl) <sub>3</sub> (5 mol%)	TEA	0.1 mmol	4.0	89.3	4.2	0.3	1.5	0.2	0.5

General reaction conditions: CuI (10 mol%), dry THF (6 mL), base (3 mL), 60 °C, 18 h; TEA = triethylamine, DIPA = diisopropylamine.

Functionalization of the B:NCD surfaces employing Sonogashira cross-coupling resulted in similar chemical surface compositions, regardless of the catalyst system, base and concentration. For all substrates, distinct S 2p and even S 2s signals were detected in the XPS survey spectra. The latter were not observed in the case of functionalization via Stille reactions, which can be seen in Figure 3, where both reactions are being compared. Deconvolution of the S 2p peaks and comparison with other reports confirmed that the sulfur signal is consistent with that for thiophene.<sup>58</sup> Furthermore, in the case of the Sonogashira cross-coupling, the relative atomic concentrations of Pd and Cu on the surface are very low (< 1 at.%). Combined with the detection of the B 1s signal, it can safely be assumed that relatively thin organic layers with minor surface contamination are obtained. Actual cross-coupling was confirmed by performing a control experiment where Pd and CuI were excluded (Figure S1). It is worth mentioning that after Sonogashira cross-coupling, the I 3d peak is still present and reaches concentrations up to 0.5 at.%, which is similar to the values obtained after diazonium grafting of 4-iodoaniline. The presence of this signal is most likely a combination of residual iodine from the CuI co-catalyst and remaining iodophenyl groups on the diamond

surface, which have not reacted. Finally, successful Sonogashira cross-coupling was confirmed by oxidation of the thiophene molecules present on the surface, as previously demonstrated by Wang *et al.* (see Figure S2).<sup>59</sup>

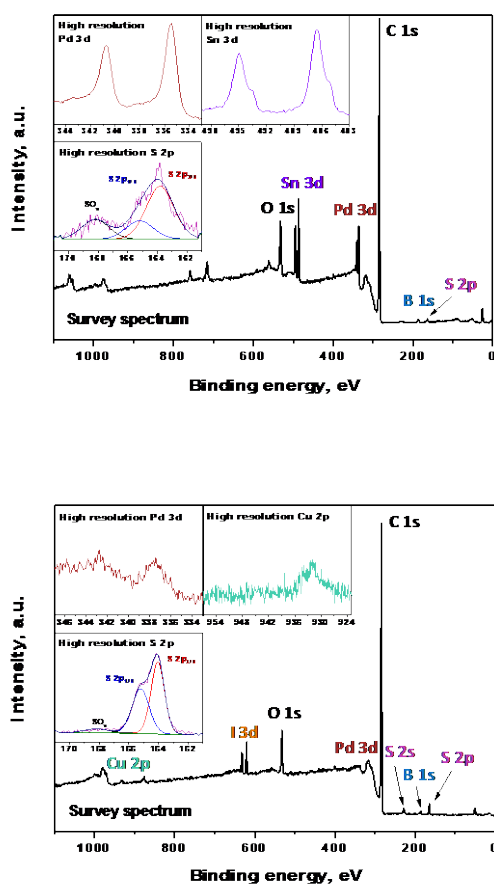


**Figure 3.** Comparison of the XPS spectra for the Stille (top; Table 1, entry 3) and Sonogashira cross-coupling (bottom; Table 4, entry 2) on a B:NCD thin film.

## 4. Conclusions

In summary, we have demonstrated successful electrochemical diazonium grafting of a thin iodophenyl layer on H-terminated boron-doped nanocrystalline diamond thin films via *in situ* diazotization of 4-iodoaniline. Optimization of the Pd-catalyzed Stille cross-coupling provided fundamental insights on the negative influence of both sterically hindered reagents and catalysts for further diamond surface functionalization. By employing a combination of 2-

(trimethylstannyl)thiophene as reagent and Pd<sub>2</sub>dba<sub>3</sub> / P(*o*-tolyl)<sub>3</sub> as catalyst system, a surface coverage of 1.0 at.% S was obtained. However, due to the formation of (thick) contamination layers and stability issues with the organostannyl derivatives, this reaction seems little suitable for the development of real diamond based devices toward sensing or photovoltaic applications. On the other hand, the Sonogashira cross-coupling afforded an average surface coverage of 2.0 at.% S, whereas the relative atomic concentration of any surface contaminant was considerably smaller (< 0.5 at.%) than for the Stille cross-coupling. Similar results were obtained, regardless of the employed catalyst system and concentration, proving the robustness of the reaction. As a result, the Sonogashira reaction is currently being investigated for the coupling of donor-acceptor type light-harvesting molecules to B:NCD thin films with the perspective of developing ‘all carbon’ hybrid photovoltaics.

## Supporting Information

XPS data on the diazonium grafting of 4-iodoaniline, alternative Stille cross-coupling protocol, XPS survey spectrum of the Sonogashira control experiment, cyclic voltammograms showing oxidation of the coupled thiophene molecules, and experimental details on the growth of boron-doped diamond on Si and Au substrates.

## Author Information

### Corresponding authors:

\*E-mail: [wouter.maes@uhasselt.be](mailto:wouter.maes@uhasselt.be)

Phone: +32-11-268312

\*E-mail: [rezek@fzu.cz](mailto:rezek@fzu.cz)

Phone: +420 22435 2330

## Acknowledgements

The authors thank UHasselt, the Research Foundation – Flanders (FWO Vlaanderen), the Czech Science Foundation project 15-01809S and the European Regional Development Fund project CZ.02.1.01/0.0/0.0/15 003/0000464 for financial support. J. Raymakers thanks the FWO for his PhD fellowship.

## References

1. Kobashi, K.; Nishimura, K.; Kawate, Y.; Horiuchi, T. Synthesis of Diamonds by Use of Microwave Plasma Chemical-Vapor Deposition: Morphology and Growth of Diamond Films. *Phys. Rev. B* **2009**, *38*, 4067-4084.
2. Nemanich, R. J.; Carlisle, J. A.; Hirata, A.; Haenen, K. CVD Diamond - Research, Applications, and Challenges. *MRS Bull.* **2014**, *39*, 490-494.
3. Szunerits, S.; Nebel, C. E.; Hamers, R. J. Surface Functionalization and Biological Applications of CVD Diamond. *MRS Bull.* **2014**, *39*, 517-524.
4. Lim, C. H. Y. X.; Zhong, Y. L.; Janssens, S.; Nesládek, M.; Loh, K. P. Oxygen-Terminated Nanocrystalline Diamond Film as an Efficient Anode in Photovoltaics. *Adv. Funct. Mater.* **2010**, *20*, 1313-1318.
5. Janssens, S. D.; Pobedinskas, P.; Vacík, J.; Petráková, V.; Ruttens, B.; D'Haen, J.; Nesládek, M.; Haenen, K.; Wagner, P. Separation of Intra- and Intergranular Magnetotransport Properties in Nanocrystalline Diamond Films on the Metallic Side of the Metal-Insulator Transition. *New J. Phys.* **2011**, *13*, 83008.
6. Macpherson, J. V. A Practical Guide to Using Boron Doped Diamond in Electrochemical Research. *Phys. Chem. Chem. Phys.* **2015**, *17*, 2935-2949.

7. Stotter, J.; Show, Y.; Wang, S.; Swain, G. Comparison of the Electrical, Optical, And Electrochemical Properties of Diamond and Indium Tin Oxide Thin-Film Electrodes. *Chem. Mater.* **2015**, *17*, 4880-4888.
8. Tang, L.; Tsai, C.; Gerberich, W. W.; Kruckeberg, L.; Kania, D. R. Biocompatibility of Chemical-Vapour-Deposited Diamond. *Biomaterials* **1995**, *16*, 483-488.
9. Yang, N.; Foord, J. S.; Jiang, X. Diamond Electrochemistry at the Nanoscale: A Review. *Carbon* **2016**, *99*, 90-110.
10. Hupert, M.; Muck, A.; Wang, J.; Stotter, J.; Cvackova, Z.; Haymond, S.; Show, Y.; Swain, G. M. Conductive Diamond Thin-films in Electrochemistry. *Diam. Relat. Mater.* **2003**, *12*, 1940-1949.
11. Ivandini, S. T. A.; Einaga, Y. Polycrystalline Boron-Doped Diamond Electrodes for Electrocatalytic and Electrosynthetic Applications. *Chem. Commun.* **2017**, *53*, 1338-1347.
12. Reitinger, A. A.; Hutter, N. A.; Donner, A.; Steenackers, M.; Williams, O. A.; Stutzmann, M.; Jordan, R.; Garrido, J. A. Functional Polymer Brushes on Diamond as a Platform for Immobilization and Electrical Wiring of Biomolecules. *Adv. Funct. Mater.* **2013**, *23*, 2979-2986.
13. Subramanian, P.; Motorina, A.; Yeap, W. S.; Haenen, K.; Coffinier, Y.; Zaitsev, V.; Niedziolka-Jonsson, J.; Boukherroub, R.; Szunerits, S. An Impedimetric Immunosensor Based on Diamond Nanowires Decorated with Nickel Nanoparticles. *Analyst* **2014**, *139*, 1726-1731.
14. Härtl, A.; Schmich, E.; Garrido, J. A.; Hernando, J.; Catharino, S. C. R.; Walter, S.; Feulner, P.; Kromka, A.; Steinmüller, D.; Stutzmann, M. Protein-Modified Nanocrystalline Diamond Thin Films for Biosensor Applications. *Nat. Mater.* **2004**, *3*, 736-742.



15. Volpe, P.; Pernot, J.; Muret, P.; Omnès, F. High Hole Mobility in Boron Doped Diamond for Power Device Applications. *Appl. Phys. Lett.* **2009**, *94*, 92102.
16. Zhong, Y. L.; Midya, A.; Ng, Z.; Chen, Z. K.; Daenen, M.; Nesladek, M.; Loh, K. P. Diamond-Based Molecular Platform for Photoelectrochemistry. *J. Am. Chem. Soc.* **2008**, *130*, 17218-17219.
17. Rezek, B.; Cermak, J.; Kromka, A.; Ledinský, M.; Hubík, P.; Mares, J.; Purkrt, A.; Cimrová, V.; Fejfar, A.; Kocka, J. Properties of Organic-Based Nanoscale Heterojunctions. *Nanoscale Res. Lett.* **2011**, *6*, 238-249.
18. Wang, J.; Firestone, M. A.; Auciello, O.; Carlisle, J. A. Surface Functionalization of Ultrananocrystalline Diamond Films by Electrochemical Reduction of Aryldiazonium Salts. *Langmuir* **2004**, *20*, 11450-11456.
19. Pinson, J.; Podvorica, F. Attachment of Organic Layers to Conductive or Semiconductive Surfaces by Reduction of Diazonium Salts. *Chem. Soc. Rev.* **2005**, *34*, 429-439.
20. Sayed, S. Y.; Bayat, A.; Kondratenko, M.; Leroux, Y. R.; Hapiot, P.; McCreery, R. L. Bilayer Molecular Electronics: All-Carbon Electronic Junctions Containing Molecular Bilayers Made with 'Click' Chemistry. *J. Am. Chem. Soc.* **2013**, *135*, 12972-12975.
21. Wang, X.; Landis, E. C.; Franking, R.; Hamers, R. J. Surface Chemistry for Stable and Smart Molecular and Biomolecular Interfaces via Photochemical Grafting of Alkenes. *Acc. Chem. Res.* **2010**, *43*, 1205-1215.
22. Wang, X.; Colavita, P. E.; Streifer, J. A.; Butler, J. E.; Hamers, R. J. Photochemical Grafting of Alkenes onto Carbon Surfaces: Identifying the Roles of Electrons and Holes. *J. Phys. Chem. C* **2010**, *114*, 4067-4074.
23. Bogdanowicz, R.; Sawczak, M.; Niedzialkowski, P.; Zieba, P.; Finke, B.; Ryl, J.; Karczewski, J.; Ossowski, T. Novel Functionalization of Boron-Doped Diamond by

- Microwave Pulsed-Plasma Polymerized Allylamine Film. *J. Phys. Chem. C* **2014**, *118*, 8014-8025.
24. Nakamura, T.; Ohana, T. Surface Functionalization of Diamond Films by Photoreaction of Elemental Sulfur and Their Surface Properties. *Jpn. J. Appl. Phys.* **2012**, *51*, 85201.
  25. Yeap, W. S.; Liu, X.; Bevk, D.; Pasquarelli, A.; Lutsen, L.; Fahlman, M.; Maes, W.; Haenen, K. Functionalization of Boron-Doped Nanocrystalline Diamond with N3 Dye Molecules. *ACS Appl. Mater. Interfaces* **2014**, *6*, 10322-10329.
  26. Meziane, D.; Barras, A.; Kromka, A.; Houdkova, J.; Boukherroub, R.; Szunerits, S. Thiol-yne Reaction on Boron-Doped Diamond Electrodes: Application for the Electrochemical Detection of DNA-DNA Hybridization Events. *Anal. Chem.* **2012**, *84*, 194-200.
  27. Yao, S. A.; Ruther, R. E.; Zhang, L.; Franking, R. A.; Hamers, R. J.; Berry, J. F. Covalent Attachment of Catalyst Molecules to Conductive Diamond: CO<sub>2</sub> Reduction using 'Smart' Electrodes. *J. Am. Chem. Soc.* **2012**, *134*, 15632-15635.
  28. Yeap, W. S.; Murib, M. S.; Cuypers, W.; Liu, X.; van Grinsven, B.; Ameloot, M.; Fahlman, M.; Wagner, P.; Maes, W.; Haenen, K. Boron-Doped Diamond Functionalization by an Electrografting/Alkyne-Azide Click Chemistry Sequence. *ChemElectroChem* **2014**, *1*, 1145-1154.
  29. Natsui, K.; Yamamoto, T.; Akahori, M.; Einaga, Y. Photochromism-Induced Amplification of Critical Current Density in Superconducting Boron-Doped Diamond with an Azobenzene Molecular Layer. *ACS Appl. Mater. Interfaces* **2015**, *7*, 887-894.
  30. Zhong, Y. L.; Loh, K. P.; Midya, A.; Chen, Z. Suzuki Coupling of Aryl Organics on Diamond. *Chem. Mater.* **2008**, *20*, 3137-3144.
  31. Zhong, Y. L.; Loh, K. P. The Chemistry of C-H Bond Activation on Diamond. *Chem. An Asian J.* **2010**, *5*, 1532-1540.

32. Kato, H.; Hees, J.; Hoffmann, R.; Wolfer, M.; Yang, N.; Yamasaki, S.; Nebel, C. E. Diamond Foam Electrodes for Electrochemical Applications. *Electrochem. Commun.* **2013**, *33*, 88-91.
33. Yu, Y.; Wu, L.; Zhi, J. Diamond Nanowires: Fabrication, Structure, Properties, and Applications. *Angew. Chem. Int. Ed.* **2014**, *53*, 14326-14351.
34. Petrak, V.; Vlckova Zivcova, Z.; Krýsov, H.; Frank, O.; Kope, J.; Taylor, A.; Kavan, L.; Mortet, V. Fabrication of Porous Boron-Doped Diamond on SiO<sub>2</sub> Fiber Templates. *Carbon* **2017**, *114*, 457-464.
35. Yeap, W. S.; Bevk, D.; Liu, X.; Krysova, H.; Pasquarelli, A.; Vanderzande, D.; Lutsen, L.; Kavan, L.; Fahlman, M.; Maes, W. *et al.* Diamond Functionalization with Light-Harvesting Molecular Wires: Improved Surface Coverage by Optimized Suzuki Cross-Coupling Conditions. *RSC Adv.* **2014**, *4*, 42044-42053.
36. Krysova, H.; Vlckova-zivcova, Z.; Barton, J.; Petrak, V.; Nesladek, M.; Cigler, P.; Kavan, L. Visible-Light Sensitization of Boron-Doped Nanocrystalline Diamond Through Non-Covalent Surface Modification. *Phys. Chem. Chem. Phys.* **2014**, *17*, 1165-1172.
37. Krysova, H.; Barton, J.; Petrak, V.; Jurok, D. R.; Kuchar, M.; Cigler, P.; Kavan, L. Efficiency and Stability of Spectral Sensitization of Boron-Doped-Diamond Electrodes Through Covalent Anchoring of a Donor-Acceptor Organic Chromophore (P1). *Phys. Chem. Chem. Phys.* **2016**, *2*, 16444-16450.
38. Krysova, H.; Kavan, L.; Zivcova, V; Yeap, W. S.; Verstappen, P.; Maes, W.; Haenen, K.; Gao, F.; Nebel, C. E. Dye-Sensitization of Boron-doped Diamond Foam: Champion Photoelectrochemical Performance of Diamond Electrodes under Solar Light Illumination. *RSC Adv.* **2015**, *5*, 81069-81077.

39. Odobel, F.; Pellegrin, Y.; Gibson, E. A.; Hagfeldt, A.; Smeigh, A. L.; Hammarström, L. Recent Advances and Future Directions to Optimize the Performances of p-Type Dye-Sensitized Solar Cells. *Coord. Chem. Rev.* **2012**, *256*, 2414-2423.
40. Bonomo, M.; Sabuzi, F.; Carlo, A. D.; Conte, V.; Dini, D.; Galloni, P. KuQuinones as Sensitizers for NiO based p-Type Dye-Sensitized Solar Cells. *New J. Chem.* **2017**, *41*, 2769-2779.
41. Mathew, S.; Yella, A.; Gao, P.; Humphry-Baker, R.; Curchod, B. F. E.; Ashari-Astani, N.; Tavernelli, I.; Rothlisberger, U.; Nazeeruddin, M. K.; Grätzel, M. Dye-Sensitized Solar Cells with 13% Efficiency Achieved through the Molecular Engineering of Porphyrin Sensitizers. *Nat. Chem.* **2014**, *6*, 242-247.
42. Espinet, P.; Echavarren, A. M. The Mechanisms of the Stille Reaction. *Angew. Chem. Int. Ed.* **2004**, *43*, 4704-4734.
43. Po, R.; Bianchi, G.; Carbonera, C.; Pellegrino, A. 'All That Glitters is not Gold': An Analysis of the Synthetic Complexity of Efficient Polymer Donors for Polymer Solar Cells. *Macromolecules* **2015**, *48*, 453-461.
44. Chinchilla, R.; Najera, C. Recent Advances in Sonogashira Reactions. *Chem. Soc. Rev.* **2011**, *40*, 5084-5121.
45. Livi, F.; Gobalasingham, N. S.; Thompson, B. C.; Bundgaard, E. Analysis of Diverse Direct Arylation Polymerization (DAP) Conditions Toward the Efficient Synthesis of Polymers Converging with Stille polymers in Organic Solar Cells. *J. Polym. Sci. Part A: Polym. Chem.* **2016**, *54*, 2907-2918.
46. Drijkoningen, S.; Janssens, S. D.; Pobedinskas, P.; Koizumi, S.; Van Bael, M. K.; Haenen, K. The Pressure Sensitivity of Wrinkled B-doped Nanocrystalline Diamond Membranes. *Sci. Rep.* **2016**, *6*, 35667.

47. Ghodbane, S.; Ballutaud, D.; Omnès, F.; Agnès, C. Comparison of the XPS Spectra from Homoepitaxial {111}, {100} and Polycrystalline Boron-Doped Diamond Films. *Diam. Relat. Mater.* **2010**, *19*, 630-636.
48. Han, C.; Bo, X.; Zhang, Y.; Li, M.; Guo, L. One-Pot Synthesis of Nitrogen and Sulfur Co-doped Onion-like Mesoporous Carbon Vesicle as an Efficient Metal-Free Catalyst for Oxygen Reduction Reaction in Alkaline Solution. *J. Power Sources* **2014**, *272*, 267-276.
49. Jiang, S.; Sun, Y.; Dai, H.; Hu, J.; Ni, P.; Wang, Y.; Li, Z. Facile Synthesis of Nitrogen and Sulfur Dual-doped Hierarchical Micro/Mesoporous Carbon Foams as Efficient Metal-free Electrocatalysts for Oxygen Reduction Reaction. *Electrochim. Acta* **2015**, *175*, 826-836.
50. Leroux, Y. R.; Hapiot, P. Nanostructured Monolayers on Carbon Substrates Prepared by Electrografting of Protected Aryldiazonium Salts. *Chem. Mater.* **2013**, *25*, 489-495.
51. Cumpson, P. J.; Seah, M. P. Elastic Scattering Corrections in AES and XPS. II. Estimating Attenuation Lengths and Conditions Required for Their Valid Use in Overlayer/Substrate Experiments. *Surf. Interface Anal.* **1997**, *25*, 430-446.
52. Nebel, C. E.; Shin, D.; Rezek, B.; Tokuda, N.; Uetsuka, H.; Watanabe, H. Diamond and Biology. *J. R. Soc. Interface* **2007**, *4*, 439-461.
53. Socrates, G. Infrared and Raman Characteristic Group Frequencies: Tables and Charts, John Wiley & Sons, Chichester, **2007**.
54. Pearlman, B. A.; Putt, S. R.; Fleming, J. A. Olefin Synthesis by Reaction of Stabilized Carbanions with Carbene Equivalents. *J. Org. Chem.* **1985**, *50*, 3622-3624.
55. Barder, T. E.; Walker, S. D.; Martinelli, J. R.; Buchwald, S. L. Catalysts for Suzuki-Miyaura Coupling Processes: Scope and Studies of the Effect of Ligand Structure. *J. Am. Chem. Soc.* **2005**, *127*, 4685-4696.

56. Naber, J. R.; Buchwald, S. L. Palladium-Catalyzed Stille Cross-Coupling Reaction of Aryl Chlorides Using a Pre-Milled Palladium Acetate and XPhos Catalyst System. *Adv. Synth. Catal.* **2008**, *350*, 957-961.
57. Carsten, B.; He, F.; Son, H. J.; Xu, T.; Yu, L. Stille Polycondensation for Synthesis of Functional Materials. *Chem. Rev.* **2011**, *111*, 1493-1528.
58. Sako, E. O.; Kondoh, H.; Nakai, I.; Nambu, A.; Nakamura, T.; Ohta, T. Reactive Adsorption of Thiophene on Au (1 1 1) from Solution. *Chem. Phys. Lett.* **2005**, *413*, 267-271.
59. Wang, M.; Das, M. R.; Li, M.; Boukherroub, R.; Szunerits, S. "Clicking" Thiophene on Diamond Interfaces. Preparation of a Conducting Polythiophene/Diamond Hybrid Material. *J. Phys. Chem. C* **2009**, *113*, 17082-17086.

# TOC Graphic

